

## High spatial resolution aerosol retrieval with MAIAC: Application to mountain regions

E. Emili,<sup>1,2</sup> A. Lyapustin,<sup>3</sup> Y. Wang,<sup>3,4</sup> C. Popp,<sup>5</sup> S. Korin,<sup>3,6</sup> M. Zebisch,<sup>2</sup> S. Wunderle,<sup>1</sup>  
and M. Petitta<sup>2</sup>

Received 24 May 2011; revised 6 September 2011; accepted 7 October 2011; published 15 December 2011.

[1] Aerosol spatial distribution in populated mountain areas is very heterogeneous and often characterized by scales of variability of several kilometers. Satellites provide an effective tool to map aerosols on an operational basis, but most of the aerosol products intended for continental/global applications have a coarse spatial resolution (10–18 km). The Multiangle Implementation of Atmospheric Correction (MAIAC) is a recently developed algorithm for the Moderate Resolution Imaging Spectroradiometer (MODIS), which provides Aerosol Optical Depth (AOD) at a high resolution of 1 km. We analyze the quality and potential of MAIAC AOD in the Alpine region and we derive high resolution AOD maps for the years 2008 and 2009. Cloudiness and snow in mountain regions occasionally lead to an overestimation of AOD due to unresolved cloud and snow pixel contamination. Therefore, we developed a filter that almost preserves the spatial resolution of the product to ensure the good accuracy of MAIAC AOD for air-quality and climatological applications. The AOD is validated with AERONET measurements in the region and compared to the standard MODIS AOD product (MOD04). Similar accuracies are found for both products (RMSE = 0.05) but with MAIAC providing about 50% more observations at the examined locations, because of its higher spatial resolution and less restrictive filtering. Comparison with ground measurements of aerosol mass (PM<sub>10</sub>) shows that MAIAC AOD can be used to detect the fine scales of aerosol variability (2–3 km) in the mountains. Finally, AOD maps for the Alpine region demonstrate that topography is correlated with the average aerosol spatial distribution.

**Citation:** Emili, E., A. Lyapustin, Y. Wang, C. Popp, S. Korin, M. Zebisch, S. Wunderle, and M. Petitta (2011), High spatial resolution aerosol retrieval with MAIAC: Application to mountain regions, *J. Geophys. Res.*, 116, D23211, doi:10.1029/2011JD016297.

### 1. Introduction

[2] Aerosols have an impact on the climate which is not yet well understood and quantified [*Intergovernmental Panel on Climate Change*, 2007]. Aerosols also affect human health [*Brunekreef and Holgate*, 2002] and the range of activities through alteration of visibility [*Wang et al.*, 2009]. The European Alpine region (Figure 1) is a densely populated mountain area with consistent sources of anthropogenic aerosol emissions from traffic, industries and home heating

[*Gehrig and Buchmann*, 2003]. The concentration of population and major European transport routes along the main valleys, which are relatively narrow (~2–5 km) and have rather steep mountain slopes, together with the local meteorology [*Gohm et al.*, 2009], create specific forcing conditions that result in very heterogeneous aerosol distribution with scales of variability of several kilometers. Aerosol monitoring in those regions requires data with high spatial resolution. Networks of ground-based measurements such as air-quality stations [*European Environmental Agency*, 2009] or Sun photometers [*Holben et al.*, 1998] provide accurate information (aerosol mass and optical depth/properties, respectively) at specific sites with high temporal resolution but they lack a needed continuous spatial coverage. The determination of the aerosol spatial and temporal distribution remains challenging from the modeling point of view [*Cuvelier et al.*, 2007], because of relatively short lifetimes of aerosols, high variability of species, sources, sinks and physical-chemical transformations.

[3] A rapid development of satellite sensors in the last decades allowed quantification of aerosol properties within the spatial and temporal coverage specific to polar orbiting

<sup>1</sup>Remote Sensing Group, Institute of Geography, University of Bern, Bern, Switzerland.

<sup>2</sup>Institute for Applied Remote Sensing, European Academy, Bolzano, Italy.

<sup>3</sup>NASA Goddard Space Flight Center, Greenbelt, Maryland, USA.

<sup>4</sup>GEST, University of Maryland Baltimore County, Baltimore, Maryland, USA.

<sup>5</sup>Empa, Swiss Federal Laboratories for Materials Science and Technology, Dübendorf, Switzerland.

<sup>6</sup>GESTAR, Universities Space Research Association, Columbia, Maryland, USA.

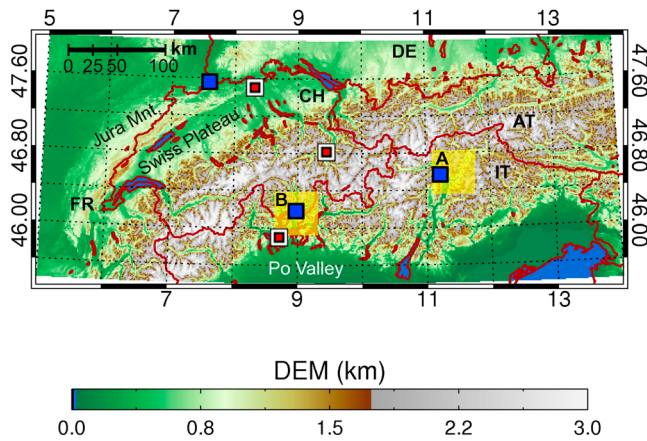


**Figure 1.** Digital Elevation Model (DEM) for the region of interest [GLOBE Task Team et al., 1999]. The red and white squares denote the location of the AERONET sites used to validate the AOD (Ispra, Davos and Laegeren from south to north). Transparent yellow boxes show two subregions enlarged in Figure 5. Blue squares denote the regions enlarged in Figure 6.

[Yu et al., 2006] and geostationary platforms [Prados et al., 2007; Popp et al., 2007]. The Moderate Resolution Imaging Spectroradiometer (MODIS) onboard the polar orbiting TERRA and AQUA satellites provides a global daily coverage at the equator per instrument and a higher coverage

toward the poles. The standard MODIS aerosol product (MOD04 for TERRA, MYD04 for AQUA) is provided by the Dark Target algorithm [Kaufman et al., 1997; Levy et al., 2007], which is complemented with the Deep Blue algorithm [Hsu et al., 2006] to allow retrievals over bright surfaces including deserts. Both these products, which have a spatial resolution of 10 km, are intended for continental/global applications. Given that the nadir resolution of MODIS bands used in the Dark Target algorithm is 500 m, the choice of 10 km resolution over land improves the MO(Y)D04 product quality by suppressing the pixel-level noise of the retrievals due to residual snow, clouds/cloud shadows, variable surface brightness etc. On the other hand, this also reduces the data coverage especially in mountain regions partially covered by snow (see Figures 2 and 3) and does not allow detecting the fine scale local emission sources or resolve inhomogeneities at scales of several kilometers, a typical width of the Alpine valleys.

[4] Data coverage is a key point for both real-time and climatological applications [Emili et al., 2010; Riffler et al., 2010]. A high spatial resolution is important where aerosols have a fine scale variability (e.g., in the Alpine valleys) and is required for the detection of aerosol sources and affected areas (traffic roads, cities).

[5] Several approaches to derive aerosol optical depth (AOD) from MODIS at high resolution have been proposed in the recent years [Chengcai et al., 2005; Wong et al., 2010]. They provide new opportunities for regional scale analysis, but application of these algorithms remains confined to a

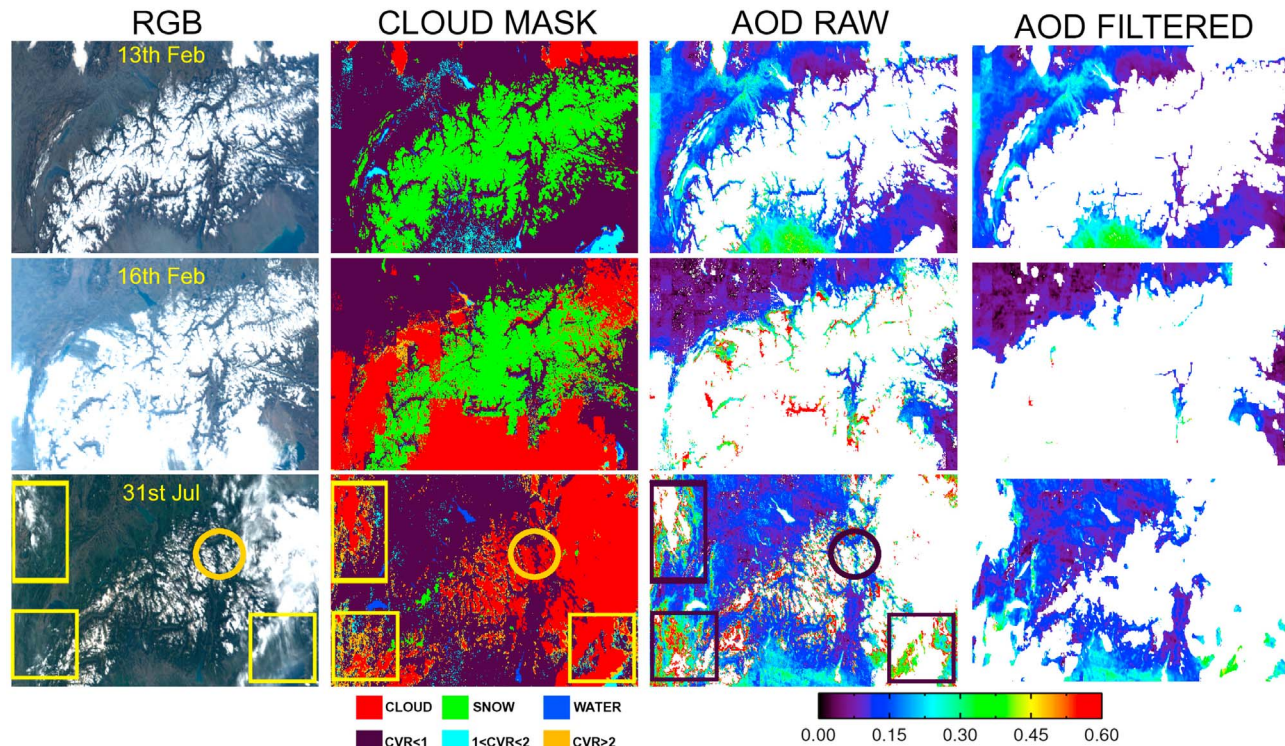


**Figure 2.** Examples of MAIAC maps for (top to bottom) three days in 2008 for the region of interest in Figure 1. From left to right: RGB image, Cloud-Snow-Water-CvR mask, MAIAC AOD ( $\lambda = 0.55 \mu\text{m}$ ), MAIAC AOD after the filtering described in Section 2.2. The boxes and circles in the third day highlight the occurrence of enhanced AOD close to clouds edges.

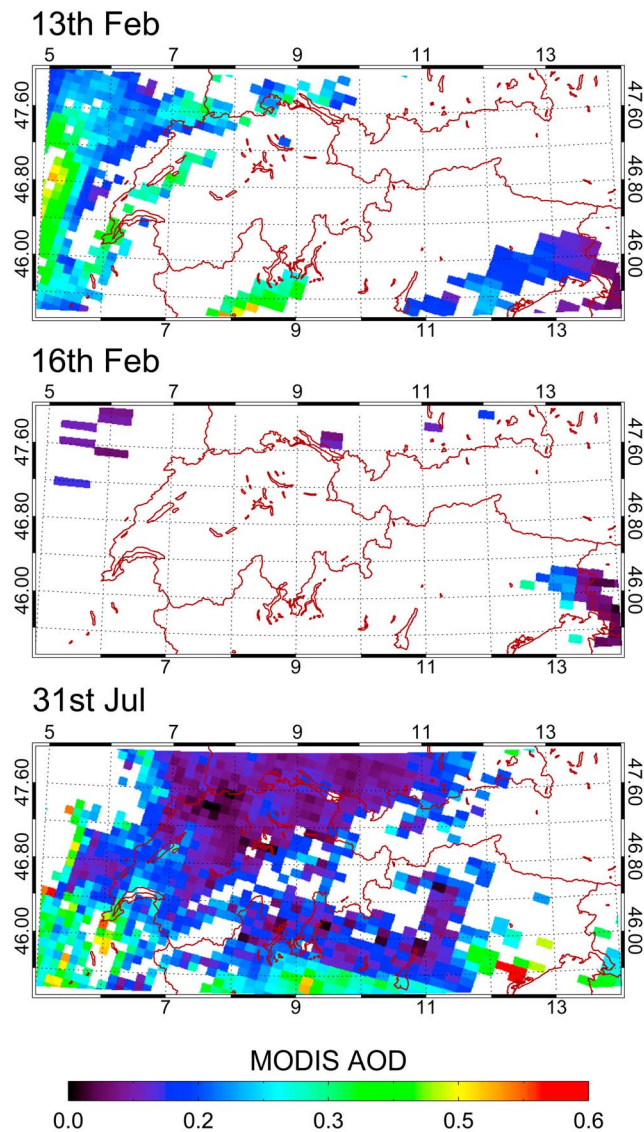


**Figure 3.** MODIS Collection 5.1 AOD (Optical Depth Land And Ocean data set) for the acquisitions in Figure 2. Lower spatial coverage than for MAIAC AOD (Figure 2) is observed during winter days while coverage is similar for both algorithms in summer.

few studies. Recently, the Multiangle Implementation of Atmospheric Correction (MAIAC) [Lyapustin *et al.*, 2011a] algorithm was developed for MODIS which performs a simultaneous retrieval of surface Bidirectional Reflection Function (BRDF) and aerosol properties at a resolution of 1 km, which is very appealing for the Alpine region (see Figure 2). This algorithm has a global scope, works over both dark and bright surfaces and it has an internal cloud mask and snow detection.

[6] In the current work we present the first applications of MAIAC data to map aerosols in the populated mountain area. We validate and apply MAIAC retrievals to compute statistics of aerosol spatial distribution in the European Alps. This study assesses the potential of high spatial resolution satellite data in regions with spatially heterogeneous aerosols.

[7] This paper is structured as follows: Section 2 introduces MAIAC products and compares MAIAC to MOD04 spatial coverage for the Alpine region. Because of unresolved clouds, snow etc., the 1 km AOD data have a higher noise in partly cloudy/snow conditions. Section 3 describes a set of filters developed for noise suppression. The direct validation of MAIAC AOD with AERONET measurements and comparison with MO(Y)D04 product for 3 mountain and valley sites is presented in Section 4. The consistency of aerosol patterns retrieved by MAIAC is also compared with ground-based aerosol mass measurements ( $PM_{10}$ ) from the spatially denser air-quality network. Finally, Section 5 describes AOD distribution along with statistics of cloud and snow cover in the Alpine area for the examined period of 2008–2009, and compares these data with available long-term statistics for the European Alps.

## 2. Data and Methods

[8] The region of interest and its topography are depicted in Figure 1. The following data have been used in this study: MAIAC products, MODIS (MOD04, MYD04) Collection 5.1 AOD [Levy *et al.*, 2007], spectral AOD from Sun photometers (AERONET) [Holben *et al.*, 1998] and ground measurements of particulate matter ( $PM_{10}$ , density of particles with a diameter smaller than  $10 \mu m$ ) from the Swiss [Schuess, 2008] and South Tyrol Environmental Agencies.

[9] The suit of MAIAC products includes cloud (cloud shadow) mask, dynamic land-water-snow mask, column water vapor, aerosol optical depth at  $0.47 \mu m$  and ratio of volumetric concentrations of the coarse and fine mode fractions (CvR) in a set of discrete values (CvR = 0, 0.6, 1.2, 2, 3, 5, e.g., CvR = 0 for pure fine mode), from which the corresponding fine mode fraction product of the Collection 5 algorithm can be computed. The aerosol models (fine and coarse modes) are specified regionally using a lognormal size distribution. The East Coast model, which is representative of continental aerosol properties (see Lyapustin *et al.* [2011a] for a detailed description), was used for the Alpine area. MAIAC land products include spectral bidirectional reflectance factor (BRF), parameters of the BRDF model and surface albedo. For the snow covered pixels, MAIAC provides a sub-pixel snow fraction and a snow grain size related to snow albedo. The products are available in a gridded format at 1 km resolution. MAIAC algorithm is based on time series analysis and combines a pixel- and imagery-level processing for fixed blocks of  $25 \times 25$  1 km pixels. The general idea behind the algorithm is that surface properties change rapidly in space and rather slowly in time, while the opposite generally holds true for the aerosols. Based on this idea, MAIAC uses up to 16 consecutive days of measurements for the fixed 25 km blocks to separate surface contribution and derive surface BRDF at 1 km resolution. With the surface BRDF known at several wavelengths, the aerosol properties are retrieved from the latest MODIS observation at 1 km resolution [Lyapustin *et al.*, 2011b, 2011a]. A similar idea is used in the MAIAC cloud mask based on the notion that the spatial structure of the image is highly reproducible in consecutive observations from space in clear-sky conditions, whereas clouds usually introduce random disturbances [Lyapustin *et al.*, 2008]. MAIAC AOD retrieval over water pixels is disregarded in this study and, if not else specified, MODIS TERRA and

AQUA data are treated without distinction. Below, both Collection 5.1 standard AOD product (Optical\_Depth\_Land\_And\_Ocean) and MAIAC AOD are considered at the wavelength of  $0.55 \mu\text{m}$ .

### 2.1. Examples of MAIAC Products

[10] Figure 2 shows three different examples of the MAIAC products including cloud/snow/CvR mask and AOD. Figure 2 (top) and Figure 2 (middle) represent two winter days, a period when stable atmospheric conditions with temperature inversion often lead to accumulation of aerosols in the shallow boundary layer. The observation geometry is close to nadir on the first day and the view angle is close to the edge of scan on the second day resulting in lower effective spatial resolution (up to 2 km). Snow cover has a wide extent on these days but low Alpine valleys appear to be snow free in the MAIAC snow mask. Figure 2 (bottom) represents a mid summer day with greener surface and reduced snow cover at high elevations. Corresponding plots of the standard MODIS Collection 5.1 AOD product for each of the three days are shown in Figure 3. The first look at the MAIAC AOD product (Figure 2, third column) reveals the potential of the high resolution data: for example, sharp and well defined boundaries are well distinguished in the aerosol distribution due to the blocking effect of topography, which during the cold seasons prevents particle transport from aerosol sources to rural elevated areas (see Figure 1). The second day features clear conditions north of the Alps and overcast conditions in the south. Notably there is a clear presence of high AOD outliers with values above 0.5 in the Alpine valleys due to undetected sub-pixel snow contamination which may be amplified by lower spatial resolution at the edge of scan. This problem, however, persists at all view geometries on the border of snow covered areas. On the summer day, high AOD values can be observed in the vicinity of clouds (see boxed regions). At 1 km resolution, they may represent thin cloud formation/dissipation layers or sub-pixel cloudy patches undetected by the cloud mask algorithm. As a rule, many of such pixels on the border with clouds also have “coarser” particles as shown by a high CvR value ( $\text{CvR} > 2$ ) whereas the typical background aerosols are characterized by  $\text{CvR} = 0 - 2$ .

[11] These examples reveal some of the difficulties inherent to AOD retrieval in regions with persistent snow and clouds, which become particularly prominent at the high spatial resolution. At coarser resolution, the MODIS standard Collection 5 algorithm relies on statistical filtering rejecting the low 20% and high 50% percentile of the histogram distribution, thus avoiding the most problematic pixels, at the cost of degraded resolution. While snow contamination is clearly a surface artifact to be removed, high optical depth close to clouds can be a consequence of unaccounted 3D radiative transfer effects near cloud edges [Wen *et al.*, 2006] or a real signal due to modification of aerosol optical properties in condensation/evaporation layers [Koren *et al.*, 2007]. For this reason, an interpretation of “problematic” pixels near the clouds clearly depends on the specific application: for the air pollution and aerosol climatology analysis, these pixels represent high AOD outliers which need to be filtered during post-processing. A comparison of MAIAC AOD with AERONET (Section 3.1) confirms an

occasional AOD overestimation along cloud and snow edges providing an additional motivation to the development of the outlier filter.

### 2.2. AOD Filtering

[12] A mixed threshold-spatial filter has been developed and applied to MAIAC AOD in this work. As mentioned before, high AOD values occur mainly in the immediate vicinity of clouds and snow. In case of undetected or sub-pixel clouds, MAIAC typically produces high CvR values, indicating effectively larger particles.

[13] Thus, the first filter rejects high CvR values ( $\text{CvR} > 2$ ). The high CvR values, shown by the orange color in the second image of each row (Figure 2), are clearly visible on 16 February and 31 July in Figure 2 around edges of thick and bright clouds. The bottom image also shows several cases of semi-transparent sub-visible clouds, marked by boxes, which were undetected by the cloud mask algorithm but were captured by the aerosol algorithm as high CvR - high AOD values.

[14] A second filter is based on the proximity to the detected clouds (or pixels with  $\text{CvR} > 2$ ) and snow. Koren *et al.* [2007] quantified the effect of enhanced AOD close to cloud borders to decay (e-folding) in  $\sim 10$  km. The CvR does not always capture undetected clouds, especially in case of low ( $< 0.4$ ) AOD (circles in Figure 2). The second filter works as follows: for each pixel, the value of AOD is rejected if the percentage of cloud/high CvR or snow in the surrounding  $15 \times 15$  ( $7 \times 7$  for snow) pixels is higher than 20% (5% for snow). The filter serves to remove pixels within  $\sim 10$  km of the detected cloud edges. The snow proximity filter similarly removes pixels contaminated by residual snow which generally occur at smaller distance from the detected snow borders ( $\sim 1-2$  km; see Figure 2).

[15] Besides CvR, the two described filters rely on the MAIAC cloud and snow mask. They will fail if the mask is not successful, which makes it necessary to introduce an additional independent filter. The third filter is based on a spatial standard deviation of AOD ( $\sigma$ ), widely used in aerosol algorithms [e.g., Popp *et al.*, 2007; Riffler *et al.*, 2010]. The  $\sigma$ -test relies on the assumption that AOD fields are spatially smooth with limited variance and that high variations are caused by the surface artifacts or undetected clouds/snow. The  $\sigma$ -test is performed as follows: for each 1 km pixel, the average AOD and its standard deviation are computed for a surrounding  $3 \times 3$  pixels window. If  $\sigma$  is lower than a fixed threshold of 0.05, the average AOD value is assigned to the pixel. If  $\sigma > 0.05$ , then the highest AOD value in  $3 \times 3$  area is removed and statistics are recomputed. The AOD of the central pixel is considered to be non-valid if more than half of pixels (highest AOD values) were removed. In this way, the AOD field is smoothed to the spatial resolution of 2–3 km, which remains significantly higher than 10 km resolution of MOD04 product but allows to effectively suppress the retrieval noise.

[16] The threshold values for the percentage of cloud/snow contamination and  $\sigma$  were established experimentally based on visual analysis of AOD images, average reduction in data coverage and statistics of matching with AERONET measurements (Section 3.1). For example, a  $\sigma$  threshold of 0.05 was found to provide the highest reduction of the

MAIAC AOD Root Mean Square Error (RMSE) without considerable reduction of the number of retrievals. Although the exact choice of the filter parameters is based on the validation statistics for the region of interest, the proposed post-processing is of interest for other regions, as demonstrated by independent validation in non-Alpine sites (Section 3.1).

[17] The resulting reduction of noise is clearly visible in Figure 2 from comparison of the original AOD with filtered AOD, shown in the third and fourth columns, respectively. The developed filter effectively removes AOD artifacts due to unresolved snow and clouds while preserving the main spatial features of the AOD field. The loss of data points as a result of filtering is between 25% and 39% of the originally retrieved AOD pixels for the three cases. Some of the high AOD pixels in the cloud formation/dissipation zone pass the filter selection (Figure 2 (middle) and Figure 2 (bottom)) because they do not satisfy the conditions of the proposed filtering. Interestingly, MOD04 Collection 5 algorithm (with standard product quality flag) also keeps those pixels (Figure 3, bottom). However, the pattern of these high AOD pixels that pass the filtering is random in space and time so that their impact can be minimized using outlier resistant statistics for the climatological averages (median and percentiles, Section 4).

### 3. Validation

#### 3.1. Comparison With AERONET

[18] Validation of satellite aerosol retrieval is commonly performed by means of direct comparison with a reference AOD retrieved by AERONET Sun photometers. The three available instruments (see Figure 1) represent a good subset for the variety of Alpine conditions: Ispra (Italy) is located in a pre-Alpine relatively flat region dominated by forest land cover and in proximity to a lake; Laegeren is located on a forested hill (800 m a.s.l.) in the north of Switzerland, surrounded by lower altitude urban and agricultural areas; Davos is situated in an Alpine valley (1500 m a.s.l.), surrounded by high mountain peaks (>2500 m a.s.l.) and Alpine land cover (grasslands and forests). The availability of AERONET Level 2.0 AOD data in the years 2008 and 2009 is above 25 days of observations for each season and site, with the exclusion of one season of data for each site, due to the calibration of the instruments. The AERONET data are available in proportion of 45% and 55% between morning and afternoon observations. Scatter plots for the collocated MAIAC, AERONET Level 2.0 and Collection 5.1 AOD are shown in Figure 4. Because the study focuses on the fine scale aerosol patterns, the single satellite pixel closest to the site's coordinates is used, whereas the standard validation approach [Ichoku, 2002] considers all pixels within ~25 km from the Sun photometer location. AERONET data are averaged within 60 min interval of the satellite overpass and are interpolated to the reference wavelength of 0.55  $\mu\text{m}$ . The spectral interpolation is performed linearly in the log-log space between the two closest wavelengths to 0.55  $\mu\text{m}$ . MAIAC provides more than twice the number of data points as compared to Collection 5.1, which is a prominent advantage for both climatological and near-real time applications. A considerable number of the MAIAC

AOD values are, however, of low quality, especially in mountainous sites with enhanced snow cover (Laegeren and Davos). Application of the developed filter reduces the available data by about 30% but also effectively removes most of the outliers. Moreover, at all sites the number of MAIAC observations remains by more than 50% higher compared to Collection 5.1 while maintaining a comparable accuracy or even improving it (Root Mean Square Error,  $\text{RMSE} < 0.05$ ). The balance between the number and quality of retrievals depends on the requirements of the given application. In this study the number of observations and their accuracy have been analyzed as a function of the filter parameters (not shown), which led to the choice of thresholds discussed in Section 2.2. The filtered AOD was also validated for 3 additional AERONET sites in central Europe (Modena, Mainz, OHP-Observatoire) to test independently the filtering procedure. This exercise revealed similar improvements like the ones found at the Alpine sites suggesting that the empirical choice of the thresholds has not only local validity.

#### 3.2. AOD Spatial Variability

[19] PM monitors are used as proxy data for AOD to qualitatively analyze MAIAC capability to retrieve fine scale AOD variations. In fact, the air-quality stations routinely measure aerosol mass ( $\text{PM}_{10}$  and  $\text{PM}_{2.5}$ ) at distances of a few kilometers in densely populated Alpine regions. The relationship between AOD and PM has been widely discussed in the literature [Hoff and Christopher, 2009] showing moderate agreement between the two quantities. Limitations occur mainly due to temporal variability of aerosol type and vertical profiles [Emili *et al.*, 2010], which restricts the application of satellite AOD to quantitatively estimate PM in the region [Emili *et al.*, 2011]. To avoid these issues, the AOD field and the  $\text{PM}_{10}$  spatial distribution were compared here independently for several events. A subset of Alpine locations have been considered for this analysis (yellow areas in Figure 1): South Tyrol is a populated and industrialized Alpine region characterized by the presence of a major highway and a dense  $\text{PM}_{10}$  monitoring network, the Ticino is situated in the southern side of the Swiss Alps and is often affected by aerosols transported from the highly polluted Italian Po valley. To avoid overestimated AOD due to clouds, only locally clear sky conditions were used in the comparison for the first days. Furthermore, because PM data represent daily averages, only relatively stable days were selected based on agreement between MAIAC AOD from TERRA and AQUA.

[20] Figure 5 shows five examples of MO(Y)D04 and MAIAC AOD retrieval (filtered) and  $\text{PM}_{10}$  daily spatial distribution in the selected areas of the domain. The available  $\text{PM}_{10}$  in-situ measurements are displayed on top of the AOD maps. The MAIAC AOD replicates the major spatial gradients of measured  $\text{PM}_{10}$ , which was as high as 30  $\mu\text{g}/\text{m}^3$  in the second and third example. Spatial correlation between the collocated values of MAIAC AOD and  $\text{PM}_{10}$  is 0.77 and 0.82 in the first and second case and the aerosol fine scale patterns resulting from the barrier of topography clearly appear at this spatial resolution. Very thin (2–3 km wide) AOD structures are observed in the first and second day along the N-S valleys, where the main highways of the region are located. The 10 km resolution of MO(Y)D04,

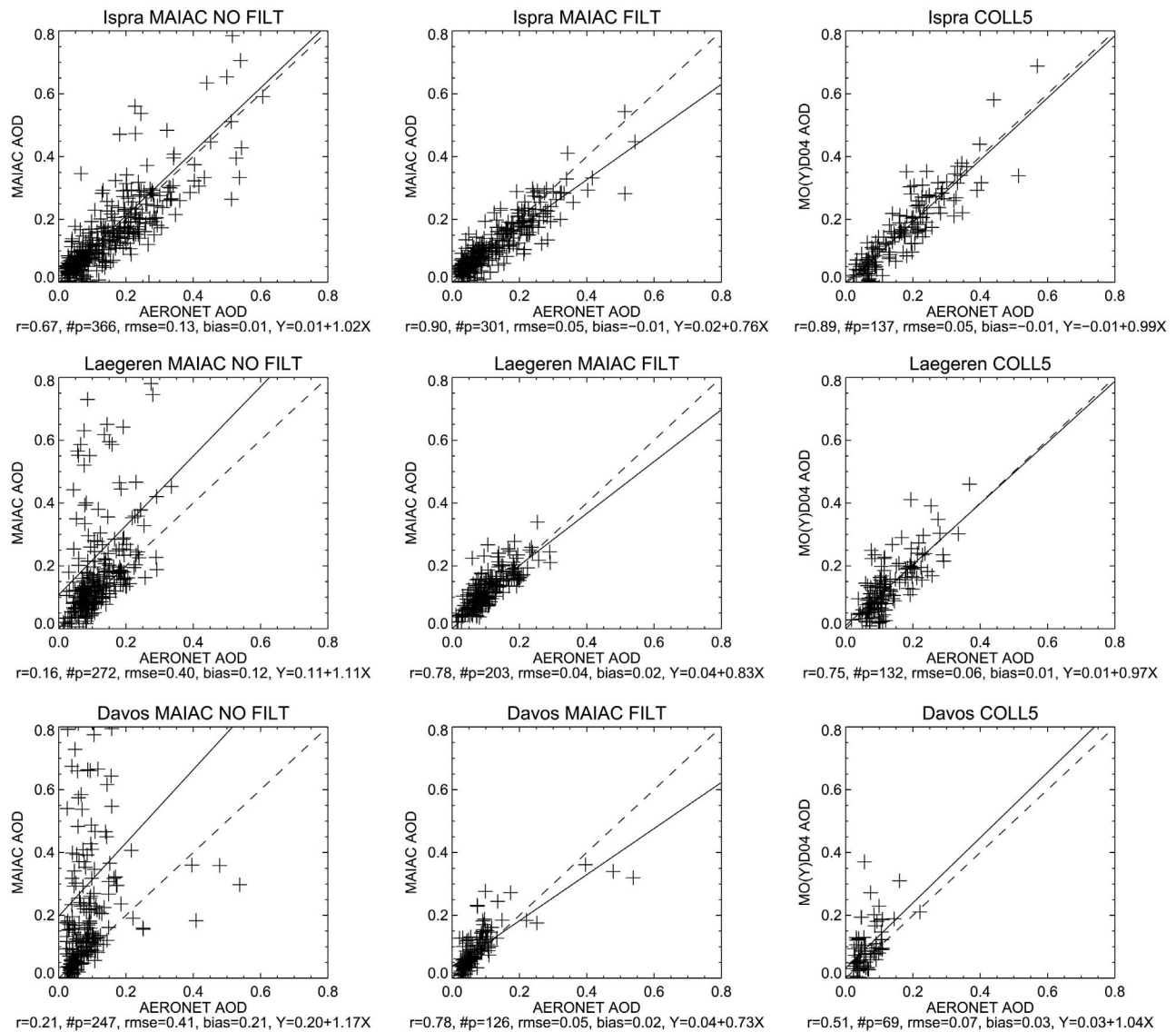


**Figure 4.** Validation scatterplots of MAIAC and Collection 5.1 AOD (AQUA and TERRA) versus AERONET Level 2.0 AOD (all at  $\lambda = 0.55 \mu\text{m}$ ) in (top to bottom) the three Alpine locations indicated in Figure 1. (left) MAIAC non filtered AOD, (middle) MAIAC filtered AOD, and (right) MODIS Collection 5. The statistics for the validation are given below each plot: correlation ( $r$ ), number of points ( $\#p$ ), root mean square error (rmse), bias and regression line.

which also shows a reduced data coverage, does not allow the local details of the AOD field to be detected (spatial correlation between MO(Y)D04 AOD and  $\text{PM}_{10}$  is  $-0.01$  and  $0.15$  for the two cases respectively). The third example shows the extension of pollution in the southern Alps, where aerosols are often transported from the southerly located and highly industrialized Po valley. The high spatial resolution permits in this case to better detect the aerosol burden. The fourth example shows a case of clear conditions, when the two  $\text{PM}$  sites also measure similar concentrations. Finally, the fifth example illustrates the difficult case of thin aerosol or thin cloud layers covering the area and is representative of partly cloudy conditions. The  $\text{PM}_{10}$  values for this day are very low on the mountain site ( $<10 \mu\text{g}/\text{m}^3$ , central pixel) whereas the AOD is not indicating such a gradient. This

demonstrates that, even after the post-processing filtering, the comparison of the AOD field with ground PM might be problematic due to elevated aerosol layers or the definition of the cloud masking (see Section 2.2). Notably, Collection 5.1 AOD does not have retrievals in the last 2 examples.

[21] Three single  $\text{PM}_{10}$  sites have been selected (blue boxes in Figure 1) to explore the AOD variability within 10 km distance (i.e. the resolution of the MOD04 product): two of them are located in populated mountain valleys with sharp topography gradients while the third is located on a relatively flat urban area (city of Basel, CH). With such selection, the effect of the topography on the aerosol annual distributions can be analyzed. Figure 6 reports the temporal average (median for 2008 and 2009) of the raw AOD and filtered AOD (second and third columns). The spatial

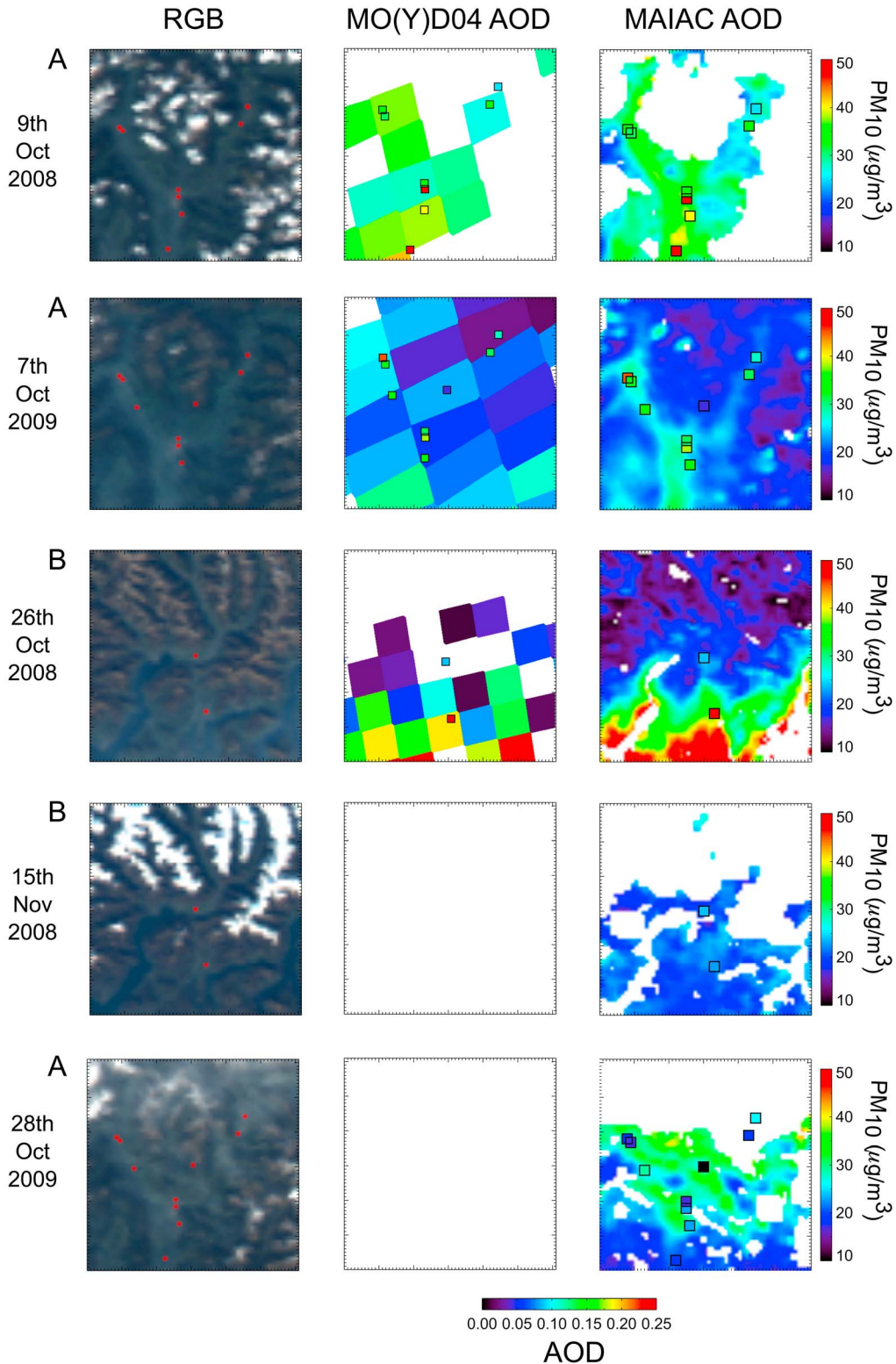


**Figure 5.** MAIAC and MO(Y)D04 AOD ( $\lambda = 0.55 \mu\text{m}$ ) distribution on five days of 2008 and 2009 at the locations indicated in Figure 1 ((top to bottom) locations A, A, B, B, and A). (left) RGB image, (middle) MO(Y)D04 AOD, and (right) MAIAC filtered AOD. The minor ticks of the map frames represent a distance of 1 km. Red pixels indicate the position of the  $\text{PM}_{10}$  measuring sites. Measured values of  $\text{PM}_{10}$  are displayed on top of the AOD maps.

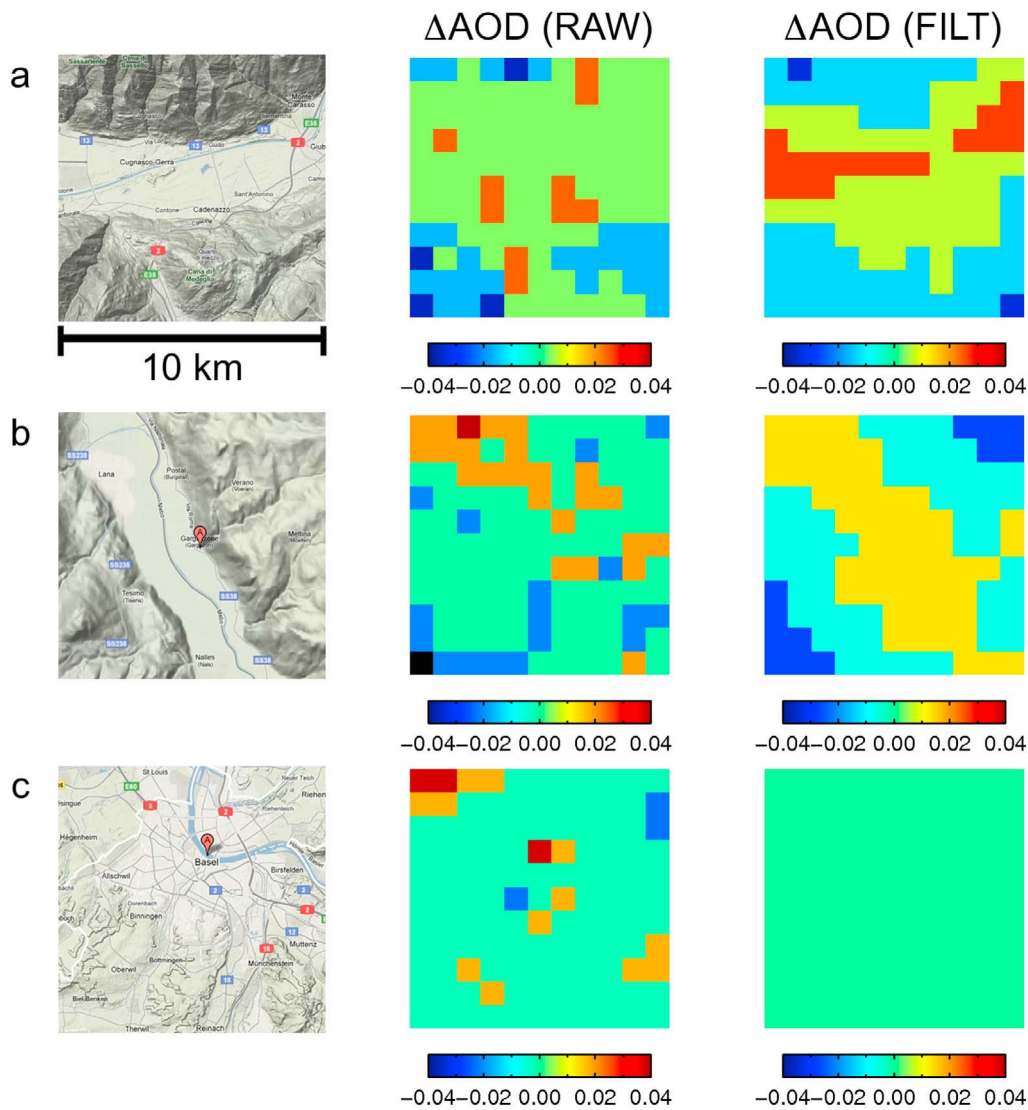


**Figure 6.** Temporal average (median for 2008 and 2009) of MAIAC AOD ( $\lambda = 0.55 \mu\text{m}$ ) at the locations indicated by the blue squares in Figure 1: (a) lower center of Figure 1, (b) right center of Figure 1, and (c) top left of Figure 1. (left) Area of interest (Copyright: 2011 Google - Map data, 2011 Google, Tele Atlas), (middle) MAIAC raw AOD, and (right) MAIAC filtered AOD. The spatial anomaly ( $\Delta$ ) is displayed instead of the absolute values to highlight spatial gradients.

anomaly ( $\Delta$ , i.e. the difference between the values at each pixel and the area average) is displayed to highlight spatial gradients in the annual averages. Figure 6 illustrates two facts: i) it emphasizes the robustness of the developed filter which allows to detect the rather low AOD signal in the valleys which otherwise is indistinguishable due to snow/cloud-related noise in the retrievals; ii) in the valleys there is significant AOD variability ( $\sim 0.1$ ) at scales  $< 10$  km and, as expected, higher AOD is found in correspondence with the valleys bottom. The third example (location c) shows that in flatter areas there are no significant spatial gradients at scales smaller than 10 km, in complete agreement with the findings of *Gehrig and Buchmann [2003]*.

[22] The evidence of AOD variability in the mountains (up to 0.1) at scales of several kilometers (typical width of

valleys) is confirmed by the satellite retrieval. These results represent, to our knowledge, the first quantitative observations of a typical mountain aerosol distribution from satellites.

#### 4. Annual and Seasonal AOD Distribution

[23] The MAIAC AOD product can be used for climate related studies, i.e. the assessment of seasonal or annual averages. One example based on two years of MODIS data (2008 and 2009) is summarized in Figure 7. The cloud and snow percentages are computed by normalization with the number of MAIAC valid pixels and AOD median values are displayed only if more than 30 (100) retrievals are available in the season (two years). Median statistics are preferable to further exclude the impact of AOD artifacts that passed the

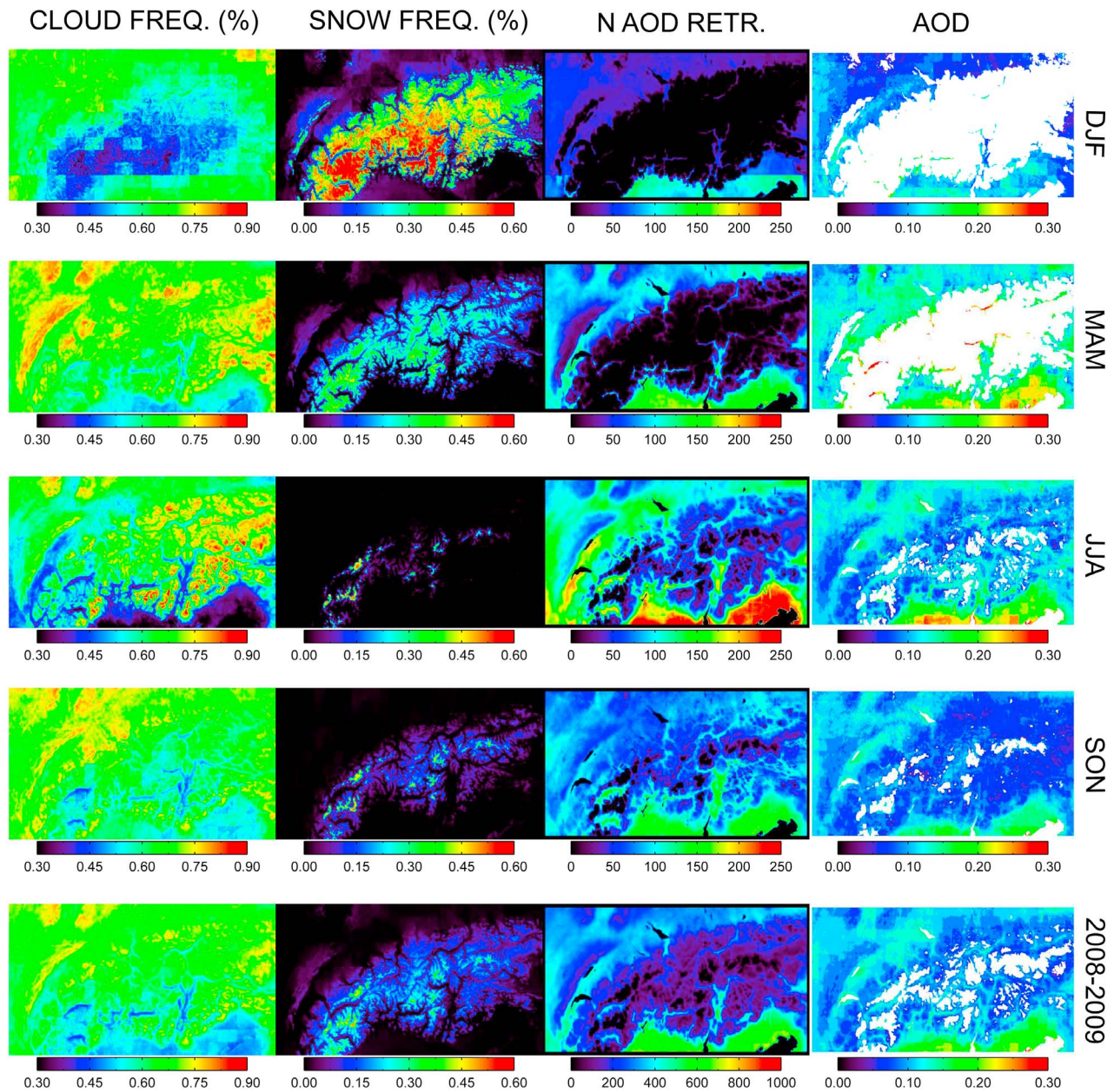


**Figure 7.** (top to bottom) Seasonal and annual statistics of MAIAC products. (left to right) Percentage of cloudy observations, snow/ice observations, number of AOD observations, and median AOD map ( $\lambda = 0.55 \mu\text{m}$ ). The percentages are computed by normalizing the number of occurrences with the total number of observations, which depends on the AQUA and TERRA orbits and viewing geometry (generally two observation per day are found but additional ones are possible near to the edges of to scan). Only points with more than 30 valid observations are shown in AOD maps (100 for the 2 years average).

filter procedure and the minimum number of valid retrievals is used to ensure the robustness of the results. The cloudiness and snow cover in the Alpine area have been previously investigated by *Kästner and Kriebel* [2001] and *Becker* [2004] using NOAA satellite data and similar results are found in this study. In DJF months elevated mountains show less than 50% cloud frequency as opposed to cloudiness of 60% in the southern side of the Alps and even higher in the northern side. During the other seasons the situation is

reversed with a minimum of 30% cloudiness in summer in the southern side of the Alps and higher than 60% on elevated mountains. A very frequent cloud coverage (75%) is found in the Swiss plateau (see Figure 1) in SON months: generally, it is always less cloudy on the southern side of the mountains.

[24] Because snow is not detected under clouds, the obtained snow maps depict the lower limit of the relative number of days with snow cover but the seasonal cycle is well captured with the winter snow frequencies higher than

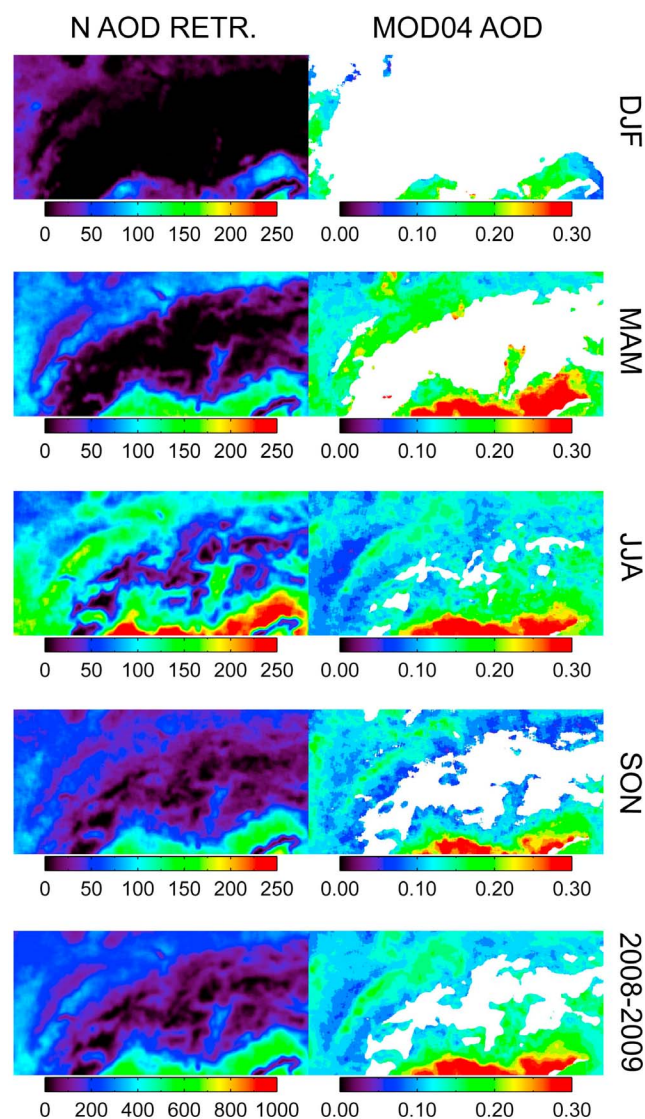


**Figure 8.** (top to bottom) Seasonal and annual statistics of Collection 5.1 AOD product. (left) Number of AOD observations and (right) median AOD map ( $\lambda = 0.55 \mu\text{m}$ ). Only points with more than 30 valid observations are shown in AOD maps (100 for the 2 years average).

10% over most of the Alpine area. The combination of snow and clouds limits the seasonal number of AQUA and TERRA AOD retrievals to  $\sim 100$ – $250$  ( $\sim 25$ – $60\%$  of the total number of observations for each season in the 2 years) on the southern side of the Alps and to  $\sim 30$ – $150$  ( $\sim 10$ – $40\%$ ) on the northern side. As expected, elevated sites (above 1 km altitude) have a non-negligible number of retrievals only during the summer and autumn. The correspondent Collection 5.1 maps are displayed in Figure 8 (left): the area average number of AOD retrievals in the Alpine region is greater for MAIAC in autumn and winter seasons and similar for the two algorithms in spring and summer seasons. Differences are generally more pronounced in Alpine valleys, whereas in flatter regions (e.g., the Po Valley) the number of retrievals is

approximately the same. This confirms the initial impression given by the examples discussed in Section 2.1 and the AERONET validation at the 3 Alpine sites (Section 3.1).

[25] The AOD spatial distribution in winter is sparse due to the reduced number of observations with median AOD values below 0.2. The AOD generally increases in spring by  $\sim 0.1$  which is correlated with the enhanced median AOD in the industrialized Po valley area (see Figure 1). A high and unrealistic AOD is found in some very narrow Alpine valleys, mostly the ones oriented in the E–W direction. A residual snow contamination is mostly responsible for this effect which is only limited to the spring season. The AOD reaches a maximum during summer and decreases again in SON months. This temporal pattern is confirmed by the AERONET data analysis. During the summer and fall seasons when the snow cover in the mountains is lowest, the effect of topography on horizontal variability of AOD with variations greater than 0.2 over distances of 3–5 km becomes obvious from MAIAC data. The two years median distribution summarizes the observed seasonal behavior: higher AOD ( $\sim 0.3$ ) is found on the Italian side of the Alps and lower one in the northern side ( $< 0.2$ ), in good agreement with previous studies [Koelemeijer *et al.*, 2006; Riffler *et al.*, 2010]. The shape of the mountain topography appears very evidently in the last AOD map (2008 and 2009). It is argued that topography is a primary factor which determines the aerosol distribution in the European Alps. In flat areas, spatial gradients in the AOD distribution of similar magnitude ( $\sim 0.1$ ) and at short scales are found only in the Po valley, but not in Switzerland close to the biggest cities. Therefore, the aerosols are well mixed horizontally in the Swiss plateau, as also confirmed by other studies [Gehrig and Buchmann, 2003; Emili *et al.*, 2010]. The correspondent Collection 5.1 maps (Figure 8, right) show that the MO(Y)D04 product captures well the coarse scale features of the AOD field in the Alps (e.g. the aerosol spread in the Swiss plateau) but do not provide as many details as MAIAC in the Alpine valleys.

## 5. Conclusions

[26] This study presents the first applications of MAIAC products to compute AOD ( $\lambda = 0.55 \mu\text{m}$ ) spatial distribution in a region where very fine scales (3–5 km) in aerosol distribution are expected. The results are summarized as follows:

[27] 1. A filtering scheme has been developed to reduce the two main sources of artifacts in MAIAC high resolution AOD from clouds and snow.

[28] 2. MAIAC AOD has similar accuracy as MODIS Collection 5.1 AOD product (RMSE  $\sim 0.05$  when compared with AERONET AOD) but provides information at 2–3 km spatial scale and with better data coverage ( $\sim 50\%$  more retrievals than Collection 5.1 at the AERONET sites) due to the higher resolution and less restrictive statistical filtering. Seasonal frequency of filtered AOD observations varies between 10–40% north of the Alps and 25–60% south of the Alps, due to combined effect of cloud and snow cover.

[29] 3. On selected days, satellite observation of spatial gradients of AOD at a local scale ( $< 10$  km) have been confirmed by the ground PM measurements.

[30] 4. Maps of high resolution AOD have been produced for the years 2008 and 2009. The main features are strong

seasonal dynamics, with AOD rising in the warm season, and evidence of significant horizontal AOD gradients (variations of 0.1 over 2–3 km) correlated with the gradients of the topography. Horizontal AOD gradients of similar intensity are also observed in flat areas, but only in the industrialized Po valley.

[31] Overall a very complex picture of aerosol distributions emerges. Consideration of these scales might be of interest for the development of regional chemical transport models and for studies about the regional radiation budget. This study demonstrates also the advantages and disadvantages of using a high resolution AOD retrieval. It is concluded that a 1 km retrieval gives valuable insights for mapping aerosol in a topographically complex terrain, provided that some care is used with cloud/snow related artifacts. Any aerosol product from current polar orbiting sensors cannot match the combination of the MAIAC sampling frequency and AOD accuracy, and this includes the current MODIS Dark Target algorithm. Sampling frequency is instead comparable between the two algorithms in flatter regions or spring–summer seasons. Frequency of observations is important for both real-time and climatological applications. Furthermore, a RMSE lower than 0.05 is desirable to investigate the spatial and temporal variability of aerosols in central Europe, where the magnitude of the AOD is less than 0.3–0.4 on average.

[32] Finally, we conclude that adapting the MAIAC AOD retrieval for the Alpine region revealed the impact of some of the major issues in AOD retrieval (e.g., the cloud/snow contamination). Consideration of the AOD post-processing ideas herein discussed are also of interest for local applications in other regions of the world. Future analysis will involve investigation of presence of temporal trends during the last 10 years of MODIS observations and local gradients of AOD in the vicinity of larger European polluted cities.

[33] **Acknowledgments.** This research was supported by the Armasuisse, Science and Technology, and the autonomous province of Bolzano (Italy). The work of A. Lyapustin, Y. Wang, and S. Korin was funded by the NASA Terrestrial Ecology Program (D. Wickland), NASA Applications Program (L. Friedl and B. Doorn), and in part by the NOAA GOES-R program (M. Goldberg). We thank the AERONET PIs for providing sun-photometers data, NABEL and APPA for providing PM10 data. We thank Lorraine Remer and two anonymous reviewers for valuable comments which helped to improve the manuscript. We also thank Armin Costa and Roberto Monsorno for the technical support.

## References

- Becker, R. (2004), Variation of snow/ice-extent and cloud coverage of the Alps as seen from NOAA operational satellites imager, *Meteorol. Z.*, *13*(3), 245–251, doi:10.1127/0941-2948/2004/0013-0245.
- Brunekreef, B., and S. T. Holgate (2002), Air pollution and health, *Lancet*, *360*(9341), 1233–1242, doi:10.1016/S0140-6736(02)11274-8.
- Chengai, L., K.-H. L. Alexis, M. Jietai, and C. D. Allen (2005), Retrieval, validation, and application of the 1-km aerosol optical depth from MODIS measurements over Hong Kong, *IEEE Trans. Geosci. Remote Sens.*, *43*(11), 2650–2658, doi:10.1109/TGRS.2005.856627.
- Cuvelier, C., P. Thunis, R. Vautard, M. Amann, B. Bessagnet, M. Bedogni, R. Berkowicz, J. Brandt, F. Brocheton, and P. Builtjes (2007), CityDelta: A model intercomparison study to explore the impact of emission reductions in European cities in 2010, *Atmos. Environ.*, *41*(1), 189–207, doi:10.1016/j.atmosenv.2006.07.036.
- Emili, E., C. Popp, M. Petitta, M. Riffler, S. Wunderle, and M. Zebisch (2010), PM10 remote sensing from geostationary SEVIRI and polar-orbiting MODIS sensors over the complex terrain of the European Alpine region, *Remote Sens. Environ.*, *114*(11), 2485–2499, doi:10.1016/j.rse.2010.05.024.
- Emili, E., C. Popp, S. Wunderle, M. Zebisch, and M. Petitta (2011), Mapping particulate matter in alpine regions with satellite and ground-based measurements: An exploratory study for data assimilation, *Atmos. Environ.*, *45*(26), 4344–4353, doi:10.1016/j.atmosenv.2011.05.051.
- European Environmental Agency (2009), Spatial assessment of PM10 and ozone concentrations in Europe (2005), *Tech. Rep. 1*, Copenhagen.
- Gehrig, R., and B. Buchmann (2003), Characterising seasonal variations and spatial distribution of ambient PM10 and PM2.5 concentrations based on long-term Swiss monitoring data, *Atmos. Environ.*, *37*(19), 2571–2580, doi:10.1016/S1352-2310(03)00221-8.
- GLOBE Task Team et al. (1999), The Global Land One-kilometer Base Elevation (GLOBE) Digital Elevation Model, Version 1.0, technical report, Natl. Oceanic and Atmos. Admin., Silver Spring, Md.
- Gohm, A., F. Harnisch, J. Vergeiner, F. Obleitner, R. Schnitzhofer, A. Hansel, A. Fix, B. Neininger, S. Emeis, and K. Schäfer (2009), Air pollution transport in an alpine valley: Results from airborne and ground-based observations, *Boundary Layer Meteorol.*, *131*(3), 441–463, doi:10.1007/s10546-009-9371-9.
- Hoff, R., and S. Christopher (2009), Remote sensing of particulate pollution from space: Have we reached the promised land?, *J. Air Waste Manage. Assoc.*, *59*(6), 645–675, doi:10.3155/1047-3289.59.6.645.
- Holben, B. N., T. F. Eck, I. Slutsker, D. Tanre, J. P. Buis, A. Setzer, E. F. Vermote, J. A. Reagan, Y. J. Kaufman, and T. Nakajima (1998), AERONET: A federated instrument network and data archive for aerosol characterization, *Remote Sens. Environ.*, *66*(1), 1–16, doi:10.1016/S0034-4257(98)00031-5.
- Hsu, N., S.-C. Tsay, M. King, and J. Herman (2006), Deep blue retrievals of Asian aerosol properties during ACE-Asia, *IEEE Trans. Geosci. Remote Sens.*, *44*(11), 3180–3195, doi:10.1109/TGRS.2006.879540.
- Ichoku, C. (2002), A spatio-temporal approach for global validation and analysis of MODIS aerosol products, *Geophys. Res. Lett.*, *29*(12), 8006, doi:10.1029/2001GL013206.
- Intergovernmental Panel on Climate Change (2007), *Contribution of Working Group I to the Fourth Assessment Report of the Intergovernmental Panel on Climate Change*, edited by S. Solomon et al., 996 pp., Cambridge Univ. Press, New York.
- Kästner, M., and K. T. Kriebel (2001), Alpine cloud climatology using long-term NOAA-AVHRR satellite data, *Theor. Appl. Climatol.*, *68*(3–4), 175–195, doi:10.1007/s007040170044.
- Kaufman, Y., D. Tanré, L. Remer, E. Vermote, A. Chu, and B. Holben (1997), Operational remote sensing of tropospheric aerosol over land from EOS moderate resolution imaging spectroradiometer, *J. Geophys. Res.*, *102*(17), 17–51.
- Koelemeijer, R., C. Homan, and J. Matthijssen (2006), Comparison of spatial and temporal variations of aerosol optical thickness and particulate matter over Europe, *Atmos. Environ.*, *40*(27), 5304–5315, doi:10.1016/j.atmosenv.2006.04.044.
- Koren, I., L. A. Remer, Y. J. Kaufman, Y. Rudich, and J. V. Martins (2007), On the twilight zone between clouds and aerosols, *Geophys. Res. Lett.*, *34*, L08805, doi:10.1029/2007GL029253.
- Levy, R. C., L. A. Remer, S. Mattoo, E. F. Vermote, and Y. J. Kaufman (2007), Second-generation operational algorithm: Retrieval of aerosol properties over land from inversion of Moderate Resolution Imaging Spectroradiometer spectral reflectance, *J. Geophys. Res.*, *112*, D13211, doi:10.1029/2006JD007811.
- Lyapustin, A., Y. Wang, and R. Frey (2008), An automatic cloud mask algorithm based on time series of MODIS measurements, *J. Geophys. Res.*, *113*, D16207, doi:10.1029/2007JD009641.
- Lyapustin, A., Y. Wang, I. Laszlo, R. Kahn, S. Korin, L. Remer, R. Levy, and J. S. Reid (2011a), Multiangle Implementation of Atmospheric Correction (MAIAC): 2. Aerosol algorithm, *J. Geophys. Res.*, *116*, D03211, doi:10.1029/2010JD014986.
- Lyapustin, A., J. Martonchik, Y. Wang, I. Laszlo, and S. Korin (2011b), Multiangle Implementation of Atmospheric Correction (MAIAC): 1. Radiative transfer basis and look-up tables, *J. Geophys. Res.*, *116*, D03210, doi:10.1029/2010JD014985.
- Popp, C., A. Hauser, N. Foppa, and S. Wunderle (2007), Remote sensing of aerosol optical depth over central Europe from MSG-SEVIRI data and accuracy assessment with ground-based AERONET measurements, *J. Geophys. Res.*, *112*, D24S11, doi:10.1029/2007JD008423.
- Prados, A. I., S. Kondragunta, P. Ciren, and K. R. Knapp (2007), GOES Aerosol/Smoke Product (GASP) over North America: Comparisons to AERONET and MODIS observations, *J. Geophys. Res.*, *112*, D15201, doi:10.1029/2006JD007968.
- Riffler, M., C. Popp, A. Hauser, F. Fontana, and S. Wunderle (2010), Validation of a modified AVHRR aerosol optical depth retrieval algorithm over central Europe, *Atmos. Meas. Tech.*, *3*(5), 1255–1270, doi:10.5194/amt-3-1255-2010.

- Schiess, M. (2008), Messresultate des Nationalen Beobachtungsnetzes für Luftfremdstoffe (NABEL), *Tech. Rep. 4*, Bundesamt für Umwelt, Bern.
- Wang, K., R. E. Dickinson, and S. Liang (2009), Clear sky visibility has decreased over land globally from 1973 to 2007, *Science*, 323(5920), 1468–1470, doi:10.1126/science.1167549.
- Wen, G., A. Marshak, and R. Cahalan (2006), Impact of 3-D clouds on clear-sky reflectance and aerosol retrieval in a biomass burning region of Brazil, *IEEE Geosci. Remote Sens. Lett.*, 3(1), 169–172, doi:10.1109/LGRS.2005.861386.
- Wong, M. S., K. H. Lee, J. E. Nichol, and Z. Li (2010), Retrieval of aerosol optical thickness using MODIS  $500 \times 500 \text{ m}^2$ , a study in Hong Kong and Pearl River Delta region, *IEEE Trans. Geosci. Remote Sens.*, 48(8), 3318–3327.
- Yu, H., et al. (2006), A review of measurement-based assessments of the aerosol direct radiative effect and forcing, *Atmos. Chem. Phys.*, 6(3), 613–666, doi:10.5194/acp-6-613-2006.
- 
- E. Emili and S. Wunderle, Remote Sensing Group, Institute of Geography, University of Bern, Hallerstrasse 12, CH-3012 Bern, Switzerland. (emanuele.emili@giub.unibe.ch)
- S. Korkin, A. Lyapustin, and Y. Wang, NASA Goddard Space Flight Center, Greenbelt, MD 20771, USA.
- M. Petitta and M. Zebisch, Institute for Applied Remote Sensing, European Academy, I-39100 Bolzano, Italy.
- C. Popp, Empa, Swiss Federal Laboratories for Materials Science and Technology, Ueberlandstrasse 129, CH-8600 Dübendorf, Switzerland.